



Fate of transient isomer of CH_2I_2 : Mechanism and origin of ionic photoproducts formation unveiled by time- resolved x-ray liquidography

Cite as: J. Chem. Phys. **150**, 224201 (2019); <https://doi.org/10.1063/1.5099002>
Submitted: 05 April 2019 . Accepted: 23 May 2019 . Published Online: 14 June 2019

Sungjun Park, Jungkweon Choi, Hosung Ki, Kyung Hwan Kim, Key Young Oang, Heegwang Roh, Joonghan Kim, Shunsuke Nozawa, Tokushi Sato, Shin-ichi Adachi, Jeongho Kim , and Hyotcherl Ihee 



View Online



Export Citation



CrossMark

ARTICLES YOU MAY BE INTERESTED IN

Accurate global potential energy surface for $\text{SiH}_2^+(X^2A_1)$ and quantum dynamics of related reaction $\text{H}(^2S) + \text{SiH}^+(X^1\Sigma^+)$

The Journal of Chemical Physics **150**, 224304 (2019); <https://doi.org/10.1063/1.5088637>

Surface morphology and straight crack generation of ultrafast laser irradiated $\beta\text{-Ga}_2\text{O}_3$

Journal of Applied Physics **125**, 223104 (2019); <https://doi.org/10.1063/1.5091700>

The microscopic Einstein-de Haas effect

The Journal of Chemical Physics **150**, 224109 (2019); <https://doi.org/10.1063/1.5092223>

Lock-in Amplifiers up to 600 MHz

starting at

\$6,210



Zurich
Instruments

Watch the Video 





Fate of transient isomer of CH₂I₂: Mechanism and origin of ionic photoproducts formation unveiled by time-resolved x-ray liquidography

Cite as: J. Chem. Phys. 150, 224201 (2019); doi: 10.1063/1.5099002

Submitted: 5 April 2019 • Accepted: 23 May 2019 •

Published Online: 14 June 2019



Sungjun Park,^{1,2,a)} Jungkweon Choi,^{2,a)} Hosung Ki,² Kyung Hwan Kim,³ Key Young Oang,⁴ Heegwang Roh,¹ Joonghan Kim,⁵ Shunsuke Nozawa,⁶ Tokushi Sato,^{6,b)} Shin-ichi Adachi,^{6,7} Jeongho Kim,^{8,c)}  and Hyotcherl Ihee^{1,2,c)} 

AFFILIATIONS

¹Department of Chemistry and KI for the BioCentury, Korea Advanced Institute of Science and Technology (KAIST), Daejeon 34141, South Korea

²Center for Nanomaterials and Chemical Reactions, Institute for Basic Science (IBS), Daejeon 34141, South Korea

³Department of Chemistry, Pohang University of Science and Technology (POSTECH), Pohang 37673, South Korea

⁴Radiation Center for Ultrafast Science, Quantum Optics Division, Korea Atomic Energy Research Institute (KAERI), Daejeon 34057, South Korea

⁵Department of Chemistry, The Catholic University of Korea, Bucheon 14662, South Korea

⁶Institute of Materials Structure Science, High Energy Accelerator Research Organization, 1-1 Oho, Tsukuba, Ibaraki 305-0801, Japan

⁷Department of Materials Structure Science, School of High Energy Accelerator Science, The Graduate University for Advanced Studies, 1-1 Oho, Tsukuba, Ibaraki 305-0801, Japan

⁸Department of Chemistry, Inha University, 100 Inha-ro, Michuhol-gu, Incheon 22212, South Korea

Note: This paper is part of the JCP special collection on Ultrafast Spectroscopy and Diffraction from XUV to X-ray.

a) Contributions: S. Park and J. Choi contributed equally to this work.

b) Present address: Center for Free-Electron Laser Science, Deutsches Elektronen Synchrotron, Notkestrasse 85, 22607 Hamburg, Germany and European XFEL GmbH, Holzkoppel 4, 22869 Schenefeld, Germany.

c) Authors to whom correspondence should be addressed: jkim5@inha.ac.kr and hyotcherl.ihee@kaist.ac.kr

ABSTRACT

Diiodomethane, CH₂I₂, in a polar solvent undergoes a unique photoinduced reaction whereby I₂⁻ and I₃⁻ are produced from its photodissociation, unlike for other iodine-containing haloalkanes. While previous studies proposed that homolysis, heterolysis, or solvolysis of *iso*-CH₂I-I, which is a major intermediate of the photodissociation, can account for the formation of I₂⁻ and I₃⁻, there has been no consensus on its mechanism and no clue for the reason why those negative ionic species are not observed in the photodissociation of other iodine-containing chemicals in the same polar solvent, for example, CHI₃, C₂H₄I₂, C₂F₄I₂, I₃⁻, and I₂. Here, using time-resolved X-ray liquidography, we revisit the photodissociation mechanism of CH₂I₂ in methanol and determine the structures of all transient species and photoproducts involved in its photodissociation and reveal that I₂⁻ and I₃⁻ are formed via heterolysis of *iso*-CH₂I-I in the photodissociation of CH₂I₂ in methanol. In addition, we demonstrate that the high polarity of *iso*-CH₂I-I is responsible for the unique photochemistry of CH₂I₂.

Published under license by AIP Publishing. <https://doi.org/10.1063/1.5099002>

INTRODUCTION

Physical and chemical properties of a molecule are governed by intramolecular forces (that is, chemical bonds) as well as

intermolecular interactions, which include dipole-dipole interaction and dispersion forces. Accordingly, the outcome of a chemical reaction is determined by such intermolecular interactions. In particular, in solution-phase reactions, the solute-solvent

interaction is a critical factor that determines the pathways and kinetics of the reaction by changing the landscape of potential energy surfaces.^{1–8} For example, there have been many reports showing that the solvent polarity alters not only the three-dimensional structure of a molecule^{9,10} but also the dynamics and mechanism of a reaction.^{11,12}

Here, we investigate an interesting photoreaction that not only exhibits the variation of reaction pathways depending on the solvent polarity but also produces a unique ionic species not observed in other photoreactions with chemical similarities. The reactant of the photoreaction, diiodomethane (CH_2I_2), is one of the most extensively investigated haloalkanes, and its photodissociation has been studied as a prototype dissociation reaction with various time-resolved techniques such as transient absorption spectroscopy,^{13–15} time-resolved resonance Raman spectroscopy,^{16–19} and time-resolved X-ray solution scattering (TRXSS).^{20,21} Figure 1 outlines various reaction pathways of CH_2I_2 photodissociation reported by several previous studies.^{13,16,20,21} Photoexcitation at 267 nm induces the $n(\text{I}) \rightarrow \sigma^*(\text{C-I})$ transition, leading to the breaking of one of the two C-I bonds in CH_2I_2 .^{14,22,23} In the gas phase, the excitation of CH_2I_2 at wavelengths longer than 248 nm generates $\text{CH}_2\text{I}\cdot$ and $\text{I}\cdot$ radical fragments.^{24–26} By contrast, in liquid solutions, the excited CH_2I_2 molecule undergoes two parallel reaction pathways: (i) radical formation, that is, dissociation of CH_2I_2 into $\text{CH}_2\text{I}\cdot$ and $\text{I}\cdot$ radicals, and (ii) isomer formation, that is, geminate recombination of $\text{CH}_2\text{I}\cdot$ and $\text{I}\cdot$ to generate *iso*- $\text{CH}_2\text{I-I}$. Both radical formation and isomer formation pathways are active irrespective of the polarity of solvent, but the ensuing reactions and their kinetics vary substantially depending on the solvent polarity, which is quite a complex photochemical behavior compared with those of other iodine-containing compounds. In nonpolar solvents, *iso*- $\text{CH}_2\text{I-I}$ undergoes homolysis to generate $\text{CH}_2\text{I}\cdot$ and $\text{I}\cdot$ radicals, and $\text{I}\cdot$ released from the solvent cage either combines nongeminately with another $\text{I}\cdot$ to form I_2 or recombines geminately/nongeminately with $\text{CH}_2\text{I}\cdot$ to regenerate CH_2I_2 . By contrast, the reaction mechanism of CH_2I_2 in polar solvents is not only more

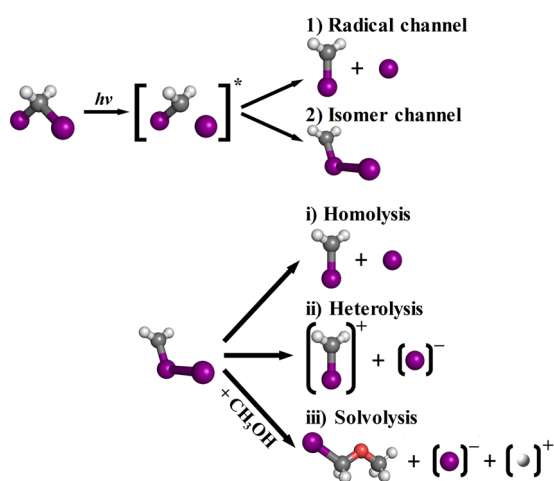


FIG. 1. Reaction pathways of CH_2I_2 photodissociation in methanol and dissociation of the isomer via homolysis, heterolysis, or solvolysis.

complicated than that in nonpolar solvents but also more complicated than the mechanisms of other iodine-containing chemicals in the same polar solvent, for example, CHI_3 , $\text{C}_2\text{H}_4\text{I}_2$, $\text{C}_2\text{F}_4\text{I}_2$, I_2 , and I_3^- .^{9–11,27–35}

The complication of the reaction mechanism of CH_2I_2 photodissociation in polar solvents stems mainly from the way how negative ionic species such as I_2^- and I_3^- are formed. Since the formation of these negative ionic species requires I^- as a precursor, the question of how I^- is formed is central to the formation mechanism of I_2^- and I_3^- but it has been controversial. From a study using ultrafast transient absorption spectroscopy, it was suggested that *iso*- $\text{CH}_2\text{I-I}$ in methanol is dissociated into CH_2I^+ and I^- via heterolysis with ion solvation.¹³ Later, based on time-resolved resonance Raman spectroscopy, nuclear magnetic resonance (NMR), and *ab initio* calculations, it was suggested that *iso*- $\text{CH}_2\text{I-I}$ undergoes solvolysis with methanol into $\text{H}^+ + \text{I}^- + \text{CH}_3\text{O-CH}_2\text{I}$, which then undergoes further solvolysis to generate $\text{CH}_3\text{O-CH}_2\text{-OCH}_3$.¹⁶ By contrast, in a study using TRXSS, it was proposed that *iso*- $\text{CH}_2\text{I-I}$ is dissociated into $\text{CH}_2\text{I}\cdot$ and $\text{I}\cdot$ via homolysis, even in polar solvents,^{20,21} and thus, electron transfer from the polar solvent to $\text{I}\cdot$ is needed for the formation of I^- . In summary, according to the previous studies, three types of dissociation pathways of *iso*- $\text{CH}_2\text{I-I}$ (that is, heterolysis, solvolysis, and homolysis) can lead to the formation of I^- , but it is still inconclusive which mechanism is in action. Here, it should be noted that, in general, the photodissociation of iodine-containing compounds such as CHI_3 , $\text{C}_2\text{H}_4\text{I}_2$, $\text{C}_2\text{F}_4\text{I}_2$, I_2 , and I_3^- results in the formation of I_2 , not I_2^- , even in the methanol solvent,^{9,10,28,32–34} indicating that the formation of I_2^- is a unique photochemical property of CH_2I_2 . Nevertheless, this point has not received proper attention in previous studies and there has been no clue for this unique photochemistry reported thus far.

To address this issue in this work, we used TRXSS to investigate the reaction dynamics of CH_2I_2 photodissociation. TRXSS, also known as time-resolved X-ray liquidography (TRXL), is a powerful tool that not only provides the information on the reaction mechanism of various chemical reactions in the solution phase but also tracks the structural progression of transient species generated during the reaction. The TRXL experiment was performed with femtosecond laser pulses (267 nm) for excitation and 100-ps X-ray pulses for probing the transient molecular structures resulting from the photodissociation of CH_2I_2 in methanol.

RESULTS AND DISCUSSION

Time-resolved difference scattering curves

The difference X-ray scattering intensities, $q\Delta S(q, t)$, containing the structural changes are shown in Fig. 2(a) as a function of the momentum transfer $q = (4\pi/\lambda)\sin\theta$, where 2θ is the scattering angle and λ is the average wavelength (0.71 Å) of the incident polychromatic X-rays with ~5% bandwidth. The difference scattering intensities were obtained by subtracting the scattering pattern measured at -3 ns (i.e., before excitation) from the scattering patterns measured at positive time delays, as described previously.^{12,32–34,36}

Figure 2 shows the experimental and theoretical $q\Delta S(q)$ curves, difference radial distribution functions (ΔRDFs), $r^2\Delta R(r)$, and the

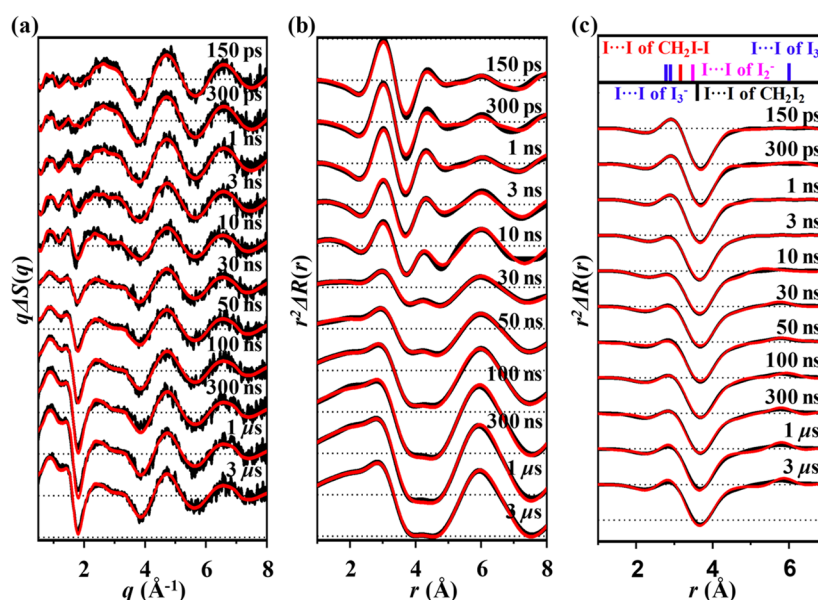


FIG. 2. Difference scattering curves, $q\Delta S(q)$, of CH_2I_2 in methanol at various time delays after excitation at 267 nm. (a) Experimental $q\Delta S(q)$ (black), where $q\Delta S(q, t) = qS(q, t) - qS(q, -3 \text{ ns})$, and calculated $q\Delta S(q)$ (red) curves based on the final optimized kinetic model. For a proper comparison of oscillatory features from 30 ns to 3 μs , $q\Delta S(q)$ below 3.4 \AA^{-1} were multiplied by a factor of 0.4. (b) The difference radial distribution function, $r^2\Delta R(r, t)$, obtained by the sine-Fourier transform of $q\Delta S(q, t)$ shown in (a). For a proper comparison of $r^2\Delta R(r, t)$, $r^2\Delta R(r, t)$ from 30 ns to 3 μs were multiplied by a factor of 0.4. (c) Experimental (black) and theoretical (red) solute-only difference radial intensity curves. The solute-related atom-atom distances are displayed at the top of the plot. The upward and downward bars with reference to a horizontal line indicate the interatomic distances of newly formed and depleted atomic pairs, respectively. The atomic pairs belonging to CH_2I_2 , $\text{CH}_2\text{I}\cdot$, I_2^- , and I_3^- are indicated in black, red, magenta, and blue, respectively.

solute-only $r^2\Delta R(r)$, that is, $r^2\Delta R_{\text{solute}}(r)$, at various time delays. Experimental difference scattering curves measured at various time delays are shown in Fig. 2(a), together with theoretical difference scattering curves that were fit to the experimental difference scattering curves using the best kinetic model, which will be discussed later. It can be seen that the experimental and the theoretical curves are in good agreement with each other, testifying the relevance of the kinetic model. In Fig. 2(b), ΔRDFs , $r^2\Delta R(r)$, obtained by sine-Fourier transform of the difference scattering curves in Fig. 2(a) are shown together with theoretical $r^2\Delta R(r)$ curves that well reproduce the experimental ones. The scattering signal of a solution sample can be decomposed into (i) the solute-only term, (ii) the cage term, and (iii) the solvent-only term. To emphasize the solute-only $r^2\Delta R(r)$, the cage and solvent-only contributions were subtracted from $r^2\Delta R(r)$ of the solution sample to obtain $r^2\Delta R_{\text{solute}}(r)$ shown in Fig. 2(c), where the internuclear distances of various solute species (that is, the reactant and reaction intermediates) involved in the photoreaction are indicated with positive (intermediate) and negative (reactant) bars.

Identification of major intermediates at 150 ps

To identify the major intermediates on subnanosecond time scale, we first analyzed the $q\Delta S(q)$ curve at 150 ps shown in Fig. 3. We considered three kinetic models of reaction pathways: (i) formation of *iso*- $\text{CH}_2\text{I}\cdot$ ($\text{CH}_2\text{I}_2 \rightarrow \text{iso-CH}_2\text{I}\cdot$), (ii) formation of CH_2I

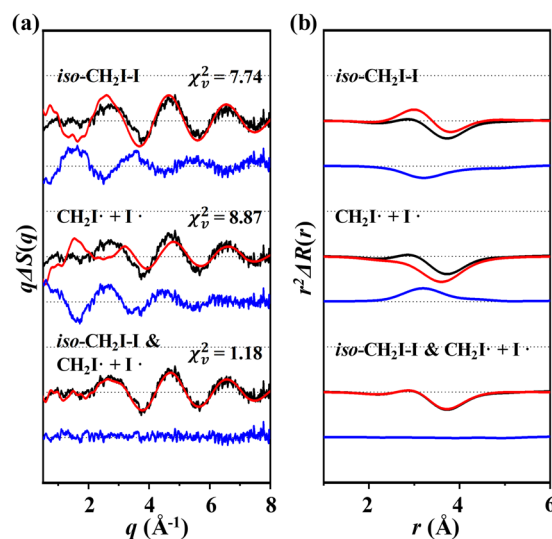


FIG. 3. Determination of reaction intermediates of CH_2I_2 photodissociation in methanol at 150 ps time delay. (a) Experimental $q\Delta S(q)$ curve at 150 ps (black) was fit by theoretical $q\Delta S(q)$ curves (red) constructed based on three kinetic models of reaction pathways: formation of only *iso*- $\text{CH}_2\text{I}\cdot$ (top), dissociation into $\text{CH}_2\text{I}\cdot$ and $\text{I}\cdot$ radicals (middle), and formation of both *iso*- $\text{CH}_2\text{I}\cdot$ and $\text{CH}_2\text{I}\cdot$ radicals (bottom). The residual (blue curves) obtained by subtracting the theoretical $q\Delta S(q)$ from the experimental $q\Delta S(q)$ is shown together. (b) $r^2\Delta R(r)$ curves obtained by the sine-Fourier transform of $q\Delta S(q)$ curves shown in (a).

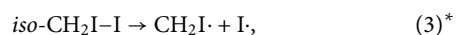
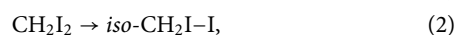
and I radicals ($\text{CH}_2\text{I}_2 \rightarrow \text{CH}_2\text{I}\cdot + \text{I}\cdot$), and (iii) formation of both $\text{CH}_2\text{I}\cdot$ and *iso*- $\text{CH}_2\text{I-I}$ with a branching ratio α [$\text{CH}_2\text{I}_2 \rightarrow (1 - \alpha)(\text{CH}_2\text{I}\cdot + \text{I}\cdot) + \alpha \text{ iso-CH}_2\text{I-I}$]. Experimental $q\Delta S(q)$ curves were fit by theoretical $q\Delta S(q)$ curves by optimizing selected structural parameters for each kinetic model. As shown in Fig. 3(a), model (iii) that includes the formation of both $\text{CH}_2\text{I}\cdot$ and *iso*- $\text{CH}_2\text{I-I}$ gives the best fit with the reduced-chi square (χ_v^2) value of 1.18 and $\alpha = 0.54 \pm 0.02$. This result suggests that the photodissociation of CH_2I_2 proceeds via the reaction pathways leading to the formation of both $\text{CH}_2\text{I}\cdot$ and *iso*- $\text{CH}_2\text{I-I}$. Previously, an optical spectroscopic study reported that *iso*- $\text{CH}_2\text{I-I}$ is formed in methanol with the quantum yield of 0.74 ± 0.08 within ~ 15 ps,¹³ whereas a previous TRXL study reported a relatively low quantum yield (0.34) for *iso*- $\text{CH}_2\text{I-I}$.^{20,21} The quantum yield for *iso*- $\text{CH}_2\text{I-I}$ obtained from our TRXL study (0.54) lies between the two previously reported values, but it is still large enough to guarantee that the *iso*- $\text{CH}_2\text{I-I}$ is a major intermediate of the photoreaction of CH_2I_2 in methanol.

The fitting analysis for the $q\Delta S(q)$ curve at 150 ps based on the three kinetic models is more intuitively visualized in the real space (that is, *r*-space), as shown in Fig. 3(b). In principle, the ΔRDF , $r^2\Delta\text{R}(r)$, obtained by the sine-Fourier-transform of $q\Delta S(q)$ gives information on the change in the distribution of interatomic distances. In ΔRDF , a positive peak indicates the formation of an atom-atom pair, whereas a negative peak corresponds to the elimination of an atom-atom pair owing to the bond cleavage. As shown in Fig. 3(b), the best-fit model, $\text{CH}_2\text{I}_2 \rightarrow 54\%$ (*iso*- $\text{CH}_2\text{I-I}$) + 46% ($\text{CH}_2\text{I}\cdot + \text{I}\cdot$), well reproduces three major features at 2.14 Å (negative), 3.09 Å (positive), and 3.60 Å (negative) in the experimental ΔRDF at 150 ps. Considering the structure of *iso*- $\text{CH}_2\text{I-I}$, the positive peak at 3.09 Å can be assigned to the formation of the I-I atomic pair in *iso*- $\text{CH}_2\text{I-I}$ and the two negative peaks at 2.14 Å and 3.60 Å correspond to the depletion of C-I and I-I atomic pairs, respectively, in CH_2I_2 by the C-I bond cleavage. As depicted in Fig. 3(b), the isomer model fails to reproduce the peak intensities in the region of 1.5–6 Å, resulting in a poor fit. Also, the radical model does not reproduce the positive peak in the region of 2–4 Å due to the absence of the isomer. These results indicate that both isomer and radicals are present at 150 ps as reaction intermediates.

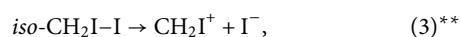
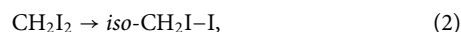
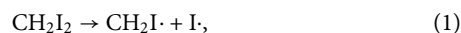
Dissociation mechanism of *iso*- $\text{CH}_2\text{I-I}$

One of the major issues investigated in this study is which reaction involving *iso*- $\text{CH}_2\text{I-I}$ is a major source of I^- , which is the precursor of I_2^- and I_3^- . The relevant reactions for three candidate kinetic models including homolysis, heterolysis, or solvolysis of *iso*- $\text{CH}_2\text{I-I}$ are as follows:

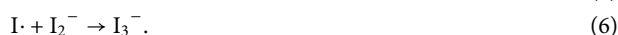
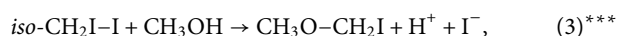
Homolysis:



Heterolysis:



Solvolysis:



The key reaction steps that are different in the three cases are emphasized with asterisks. In fact, we considered all possible pathways comprehensively, as illustrated in Fig. S1 and will be discussed later, but here, we show only the pathways that were found to be the most plausible according to the results of the global fitting (GF) analysis. In the GF analysis, the experimental difference scattering curves at all time delays were fit simultaneously by theoretical $q\Delta S(q)$ curves calculated with global fitting parameters, with the maximum likelihood estimation method being applied as a fitting algorithm. In this fitting algorithm, the χ_v^2 value for the discrepancy between the experimental and theoretical $q\Delta S(q)$ curves was employed as a measure of the goodness of the fit. The density functional theory (DFT)-optimized structures of solute molecules were used as starting structures of the global fitting and, as fitting parameters, we used several selected structural parameters of the solute molecules and other relevant kinetic parameters, for example, rate constants for all reaction pathways, branching ratios of the photoproducts, and the excitation ratio of photoexcited molecules.

In the three candidate kinetic models shown above, the products of the key reactions involving *iso*- $\text{CH}_2\text{I-I}$ are $\text{CH}_2\text{I}\cdot$, CH_2I^+ , or $\text{CH}_3\text{O-CH}_2\text{I}$. The scattering signal of $\text{CH}_3\text{O-CH}_2\text{I}$ is quite different from those of $\text{CH}_2\text{I}\cdot$ and CH_2I^+ due to extra atoms, but in principle, it is challenging to distinguish $\text{CH}_2\text{I}\cdot$ and CH_2I^+ only by their scattering patterns unless their exact three-dimensional structures are known. For example, if the atomic distances of C-I pairs, which give the largest scattering among all pairs, in those species are identical to each other, their scattering patterns will be highly similar to each other [Fig. S2(a)]. However, the cage term would still be very different depending on the absence/presence of the extra charge or extra atoms, therefore helping to distinguish $\text{CH}_2\text{I}\cdot$ and CH_2I^+ [Fig. S2(b)]. To determine the mechanism of I^- formation, we first fit experimental $q\Delta S(q)$ curves at all time delays with theoretical $q\Delta S(q)$ curves based on one of the three kinetic models: homolysis, heterolysis, and solvolysis of *iso*- $\text{CH}_2\text{I-I}$. To do so, we used the structural parameters (for CH_2I_2 , *iso*- $\text{CH}_2\text{I-I}$, $\text{CH}_2\text{I}\cdot$, CH_2I^+ , and $\text{CH}_3\text{O-CH}_2\text{I}$) predicted by DFT calculations or the experimentally reported ones (for I_2^- and I_3^-). The reduced chi-square values for the homolysis, heterolysis, and solvolysis models are 1.78, 1.67, and 1.82, respectively,

indicating that the heterolysis model gives the most satisfactory fit.

While we used the molecular structures of reaction intermediates calculated from quantum calculation to initially fit the time-resolved scattering curves, those theoretically predicted structures are not guaranteed to be accurate as the structures of intermediates involved in the nonequilibrium photochemical reaction. Therefore, we refined the structures of reaction intermediates and products by allowing all structural parameters to vary when globally fitting the experimental time-resolved scattering curves at all time delays based on each kinetic model. We assumed that the refined structure of each intermediate stays the same during the reaction. The optimized molecular structures of intermediates vary depending on the kinetic model because, in principle, each kinetic model is supposed to give different concentrations of intermediates at a given time, but the global fitting is governed by common experimental time-resolved scattering curves irrespective of the kinetic model. As the global fitting-optimized structures deviate further from the calculated structures, it is judged that the fitting is less adequate. As shown in Table I, with the refinement of the molecular structures of reaction intermediates and products, the heterolysis model still best fits the experimental $q\Delta S(q)$ curves.

To confirm which kinetic model is the most suitable, beyond the fitting quality, we also checked structural parameters such as (i) the C–I bond lengths of CH_2I^+ or $\text{CH}_2\text{I}\cdot$ and (ii) the I–I bond lengths of I_2^- , I_3^- , and *iso*- $\text{CH}_2\text{I}-\text{I}$ among the selected structural fitting parameters that were adjusted to refine the actual structure of the chemical species involved in the photodissociation of CH_2I_2 . The results show that the kinetic model including heterolysis provides the most reasonable values for the C–I bond lengths of either CH_2I^+ or $\text{CH}_2\text{I}\cdot$. As shown in Table II, for the heterolysis model, the C–I bond length of CH_2I^+ was determined to be $1.91 \pm 0.25 \text{ \AA}$, which is close to that of CH_2I^+ calculated by DFT (1.94 \AA) and CCSD(T) (1.94 \AA), and the C–I bond length of $\text{CH}_2\text{I}\cdot$ was determined to be $2.04 \pm 0.30 \text{ \AA}$, which is in excellent agreement with those of $\text{CH}_2\text{I}\cdot$ calculated by DFT (2.04 \AA) and CCSD(T)

(2.05 \AA). By contrast, for the kinetic models based on the homolysis and solvolysis, the C–I bond lengths of $\text{CH}_2\text{I}\cdot$ were determined to be $1.86 \text{ \AA} \pm 0.30$ and $1.94 \text{ \AA} \pm 0.35$, respectively, and these bond lengths are much shorter than the calculated C–I bond length value of $\text{CH}_2\text{I}\cdot$ (2.04 \AA).

However, the large uncertainty associated with the C–I bond lengths makes it difficult to judge the most suitable candidate kinetic model only based on the good agreement between the C–I bond lengths determined from the structural refinement and the DFT calculation. In this regard, the I–I bond lengths provide more convincing evidence because they would have much smaller uncertainties due to the larger scattering of I–I pairs than C–I pairs. For the I–I bond lengths of I_2^- and I_3^- , the heterolysis model again gives better agreement with the DFT-calculated values than the homolysis and solvolysis models. Specifically, with the heterolysis model, the I–I bond length of I_2^- was determined to be $3.325 \pm 0.005 \text{ \AA}$, which is close to 3.235 \AA ($\omega\text{B97X/AVTZ}$) and 3.332 \AA (MN12-SX/AVTZ) calculated from DFT calculations, whereas the homolysis and solvolysis models give the I–I bond lengths of $3.535 \pm 0.003 \text{ \AA}$ and $3.525 \pm 0.003 \text{ \AA}$, respectively, which deviate much from the DFT-calculated values.

For I_3^- , quantum calculation predicted identical bond lengths for the two I–I bonds: 2.933 \AA ($\omega\text{B97X/AVTZ}$) and 2.949 \AA (MN12-SX/AVTZ). However, according to a previous TRXL study on the photodissociation of I_3^- ,¹⁰ I_3^- formed by the reaction between I_2^- and $\text{I}\cdot$ in the polar solvent has an asymmetric structure with two different I–I bond lengths, 2.98 ± 0.03 and $3.03 \pm 0.04 \text{ \AA}$. From the global fitting analysis, the I_1-I_2 and I_2-I_3 bond lengths of I_3^- were determined to be 2.962 ± 0.012 and $3.053 \pm 0.008 \text{ \AA}$ in the heterolysis model, 2.850 ± 0.010 and $3.100 \pm 0.015 \text{ \AA}$ in the homolysis model, and 2.858 ± 0.027 and $3.066 \pm 0.023 \text{ \AA}$ in the solvolysis model, respectively. Thus, as is the case for the C–I bond lengths of CH_2I^+ or $\text{CH}_2\text{I}\cdot$ and the I–I bond length of I_2^- , the I–I bond lengths of I_3^- obtained with the heterolysis model best match the experimental values reported in the TRXL study on the photodissociation of I_3^- .¹⁰

TABLE I. Kinetic parameters for homolysis, heterolysis, and solvolysis models.

	Homolysis	Heterolysis	Solvolysis
Fraction of photoexcited molecules ^a	23.2% (± 0.2)	23.0% (± 0.1)	19.8% (± 0.1)
Fraction for the isomer channel	21.2% (± 0.4)	23.5% (± 0.5)	20.4% (± 1.1)
Fraction for the radical channel	21.9% (± 0.6)	20.0% (± 0.4)	30.1% (± 0.9)
Fraction of direct relaxation back to the ground state ^b	56.9% (± 0.1)	56.5% (± 0.2)	49.5% (± 0.1)
$\text{CH}_2\text{I}-\text{I} \rightarrow \text{CH}_2\text{I}\cdot + \text{I}\cdot$	$2.33 (\pm 0.02) \times 10^8 \text{ s}^{-1}$
$\text{CH}_2\text{I}-\text{I} \rightarrow \text{CH}_2\text{I}^+ + \text{I}^-$...	$2.23 (\pm 0.01) \times 10^8 \text{ s}^{-1}$...
$\text{CH}_2\text{I}-\text{I} + \text{CH}_3\text{OH} \rightarrow \text{CH}_3\text{OCH}_2\text{I} + \text{H}^+ + \text{I}^-$	$9.91 (\pm 0.02) \times 10^6 \text{ M}^{-1} \text{ s}^{-1}$
$\text{I}\cdot + \text{I}^- \rightarrow \text{I}_2^-$	$5.12 (\pm 0.02) \times 10^{10} \text{ M}^{-1} \text{ s}^{-1}$	$7.69 (\pm 0.03) \times 10^{10} \text{ M}^{-1} \text{ s}^{-1}$	$1.01 (\pm 0.02) \times 10^9 \text{ M}^{-1} \text{ s}^{-1}$
$\text{I}\cdot + \text{I}_2^- \rightarrow \text{I}_3^-$	$7.76 (\pm 0.01) \times 10^9 \text{ M}^{-1} \text{ s}^{-1}$	$3.28 (\pm 0.02) \times 10^{10} \text{ M}^{-1} \text{ s}^{-1}$	$1.00 (\pm 0.01) \times 10^9 \text{ M}^{-1} \text{ s}^{-1}$
Reduced chi-square ^c	1.566	1.497	1.627

^aThis value is the fraction of photoexcited molecules from the CH_2I_2 solution (50 mM) in the ground state.

^bThis value is the fraction of the photoexcited molecules that relax back to the ground state without undergoing photodissociation.

^cThe reduced chi-square value (in bold) reflects the quality of fitting. As this value is smaller, the quality of fit to the experimental data is better.

TABLE II. Optimized structural parameters of the chemical species involved in the CH₂I₂ photodissociation, obtained by either quantum chemical calculation or global fitting analysis based on homolysis, heterolysis, and solvolysis models.^a

Species	Parameter ^c	DFT		<i>Ab initio</i>	GF analysis ^b		
		ω B97X/ AVTZ ^c (methanol)	MN12-SX/ AVTZ ^d (methanol)	CCSD(T)/ AVQZ (methanol)	Homolysis	Heterolysis	Solvolysis
CH ₂ I ₂	C-I	2.125 Å	2.129 Å	2.132 Å	2.134 Å (±0.400)	2.135 Å (±0.200)	2.145 Å (±0.250)
	I-I	3.580 Å	3.585 Å	3.588 Å	3.596 Å (±0.005)	3.601 Å (±0.003)	3.625 Å (±0.002)
	I-C-I	114.76°	114.71°	114.55°	114.82° (±0.50)	114.99° (±0.35)	115.34° (±0.40)
CH ₂ I ₁ -I ₂	C-I₁	1.983 Å	1.942 Å	...	1.963 Å (±0.300)	1.975 Å (±0.250)	1.956 Å (±0.350)
	I₁-I₂	3.155 Å	3.133 Å	...	3.136 Å (±0.005)	3.094 Å (±0.006)	3.058 Å (±0.003)
	C-I₁-I₂	114.98°	121.93°	...	110.4° (±3.7)	115.7° (±4.3)	119.6° (±5.7)
CH ₂ I·	C-I	2.038 Å	2.040 Å	2.050 Å	1.864 Å (±0.300)	2.038 Å (±0.300)	1.938 Å (±0.350)
CH ₂ I ⁺	C-I	1.936 Å	1.938 Å	1.940 Å	...	1.910 Å (±0.250)	...
CH ₃ OCH ₂ I	C-I	2.208 Å	2.105 Å (±0.300)
I ₂ ⁻	I-I	3.235 Å	3.332 Å	...	3.530 Å (±0.003)	3.325 Å (±0.005)	3.525 Å (±0.027)
I ₃ ⁻ (I ₁ -I ₂ -I ₃) ⁻	I₁-I₂	2.933 Å	2.949 Å	...	2.850 Å (±0.010)	2.962 Å (±0.012)	2.858 Å (±0.027)
	I₂-I₃	2.933 Å	2.949 Å	...	3.100 Å (±0.015)	3.053 Å (±0.008)	3.066 Å (±0.023)
	I₁-I₂-I₃	180°	180°	...	180° (fixed)	180° (fixed)	180° (fixed)

^aThe listed parameters were either optimized by DFT calculations or obtained from GF analysis of the experimental TRXL data.^bErrors for global fitting parameters are shown in the parenthesis. Fixed values are excerpted from the ω B97X/AVTZ calculation.^cThe parameters (in bold) refer to the structural parameters of each chemical species. The parameters consisting of two atomic symbols represent bond lengths and the parameters consisting of three atomic symbols represent bond angles.^dDFT-optimized parameters by considering the scalar relativistic effect by introducing dhf-TZVPP small-core relativistic effective core potential (RECP) on the iodine atom.³⁷

For *iso*-CH₂I-I, with the heterolysis model, the C-I₁-I₂ angle was determined to be 115.7° ± 4.3°, which is similar to the DFT-calculated value of 114.98° (ω B97X/AVTZ) and 121.93° (MN12-SX/AVTZ). The I-I bond length of *iso*-CH₂I-I was determined to be 3.094 ± 0.006 Å, which is smaller than the DFT-calculated values, 3.155 Å (ω B97X/AVTZ) and 3.133 Å (MN12-SX/AVTZ), and larger than the experimentally determined value (3.04 Å) in a previous TRXL study on the photodissociation of CH₂I₂.^{20,21} In fact, the I-I bond length of *iso*-CH₂I-I obtained with the homolysis model is closer to the DFT values. Nevertheless, based on the global fitting of our TRXL data and the overall comparison of optimized structural parameters obtained from the fitting of experimental TRXL data with their DFT-calculated values, we conclude that the heterolysis model is the most relevant mechanism for the formation of I⁻ from *iso*-CH₂I-I.

In the previous TRXL study on CH₂I₂,^{20,21} it was found that the I-I bond length of *iso*-CH₂I-I is larger by 0.07 Å in methanol than in cyclohexane and it was suggested that the longer I-I bond length in the polar solvent originates from the stronger interaction of *iso*-CH₂I-I with methanol than with cyclohexane. In a transient absorption spectroscopy,¹³ it was shown that *iso*-CH₂I-I has a shorter lifetime (5 ns) in methanol than in *n*-hexane and it was suggested that the shorter lifetime in the polar solvent arises from the stabilization of ionic resonance forms, which may readily

undergo the heterolytic cleavage of the I-I bond. Also, CH₂I⁺ was observed in the gas-phase decomposition of CH₂I₂,^{38,39} suggesting the stability of the positive ionic species generated from heterolysis. Moreover, theoretical calculations for the products of CH₂I₂ photodissociation¹³ showed that the ion pair of CH₂I⁺ and I⁻ is stabilized significantly by the solvation in polar solvents such as methanol, ethanol, and acetonitrile and that the solvated ion pair, (CH₂I⁺ + I⁻)_{sol}, in those polar solvents has a lower energy than the radical pair of CH₂I· and I· (²P_{1/2}) [although it has a slightly higher energy than the radical pair of CH₂I· and I· (²P_{3/2})].

To examine the energetics of the three pathways for the dissociation of *iso*-CH₂I-I, we performed DFT and *ab initio* calculations for the products of CH₂I₂ photodissociation, of which the details are presented in the [supplementary material](#) and the calculation results are summarized in Fig. S3 of the [supplementary material](#). As shown in Figs. S3 and S4, the heterolysis and homolysis pathways are nearly degenerate in methanol, supporting that the heterolysis can occur in methanol in terms of energetics. Although the solvolysis pathway is an endothermic reaction that requires a lower energy than both heterolysis and homolysis pathways, the products of solvolysis, CH₃O-CH₂I and CH₃O-CH₂-OCH₃, are likely to be formed on slower time scales than the products of heterolysis and homolysis according to the result of previous time-resolved resonance

Raman study that reported the solvolysis-mediated dissociation of *iso*-CH₂I-I,¹⁶ thus negating the involvement of solvolysis in the formation of I⁻ in methanol.

Reaction kinetics

Figure 4(a) shows the time-dependent concentration profiles of chemical species involved in the photodissociation of CH₂I₂. The dissociation of *iso*-CH₂I-I occurs with the time constant of 4.48 ns, and the concentration of CH₂I⁺ increases with the same time constant, in accordance with the heterolysis mechanism. The concentration of I[·] decreases in ~10 ns via reactions (5) and (6), while I⁻ is consumed in tens of nanosecond via reaction (5). As the concentrations of I[·] and I⁻ decrease, I₂⁻ and I₃⁻ are formed until I[·] becomes depleted at ~30 ns.

In principle, I₃⁻ can be formed through reactions (5) and (6) irrespective of how *iso*-CH₂I-I is dissociated, but we can consider an alternative pathway for the formation of I₃⁻ as follows:



In a previous study on the photodissociation of CHI₃ in methanol, Lee *et al.* reported the rate constant of $3.1 \times 10^{10} \text{ M}^{-1} \text{ s}^{-1}$ for the recombination of I radicals to form I₂ in methanol.³⁴ This rate constant is smaller than that ($7.69 \times 10^{10} \text{ M}^{-1} \text{ s}^{-1}$) for reaction (5), which indicates that in methanol, the formation of I₂⁻ is kinetically favored over the formation of I₂. However, a separate simulation including reaction (7) occurring with the previously reported bimolecular rate constant shows that not only I₂⁻ but also a non-negligible amount of I₂ can be formed. To examine whether reaction (7) contributes to the photodissociation of CH₂I₂, we considered reaction (7) in all three kinetic models (that is, heterolysis, homolysis, and solvolysis). If reaction (7) is forced to occur with the previously reported bimolecular rate constant for the formation of I₂, the fit qualities deteriorate, and if the bimolecular rate constant is allowed to vary, the concentration of I₂ converges to zero,

indicating that reaction (7) is not involved. Thus, under our experimental condition, the formation of I₂ via reaction (7) does not occur and, instead, I₃⁻ is formed through reactions (5) and (6) in the photodissociation of CH₂I₂. The absence of reaction (7) is consistent with the results of previous studies using TA spectroscopy¹³ and TRXL,^{20,21} but its origin is not clear. Similarly, for the photolysis of I₃⁻, the TRXL measurement showed that reaction (7) does not occur.⁴⁰

From the GF analysis of our TRXL data, it was found that reaction (6), which occurs subsequently to reaction (5), occurs with a rate constant of $3.28 \times 10^{10} \text{ M}^{-1} \text{ s}^{-1}$. Although we found that the heterolysis model is the most suitable mechanism for the formation of I⁻ from *iso*-CH₂I-I, we tested other various kinetic models where one or more of the key reaction pathways, for example, reactions (3**), (5), and/or (6) are removed from the heterolysis model so that the significance of each removed pathway can be estimated. Removal of any pathway from the complete heterolysis model results in worse fitting of the experimental $q\Delta S(q)$ curves than fitting with the complete heterolysis model, thus confirming that each of the constituent pathways of the heterolysis model is essential. Additionally, we also tested the significance of the formation of C₂H₄I₂ by the bimolecular recombination of CH₂I[·] (CH₂I[·] + CH₂I[·] → C₂H₄I₂). Addition of this reaction step to the heterolysis kinetic model worsens the fit, confirming that this pathway is not operational within the investigated time window. We also tested a kinetic model where both heterolysis and homolysis are involved. In this case, the additional I atoms produced by homolysis should be combined to form I₂ via reaction (7), but it was already demonstrated above that the formation of I₂ was not observed in our TRXL data, indicating that reaction (7) does not occur. Therefore, we can exclude the occurrence of homolysis from the kinetic model for the photodissociation of CH₂I₂.

Comparison with other iodine-containing compounds

To explain the unique photochemical behavior of CH₂I₂ in methanol in contrast to other iodine-containing compounds, we

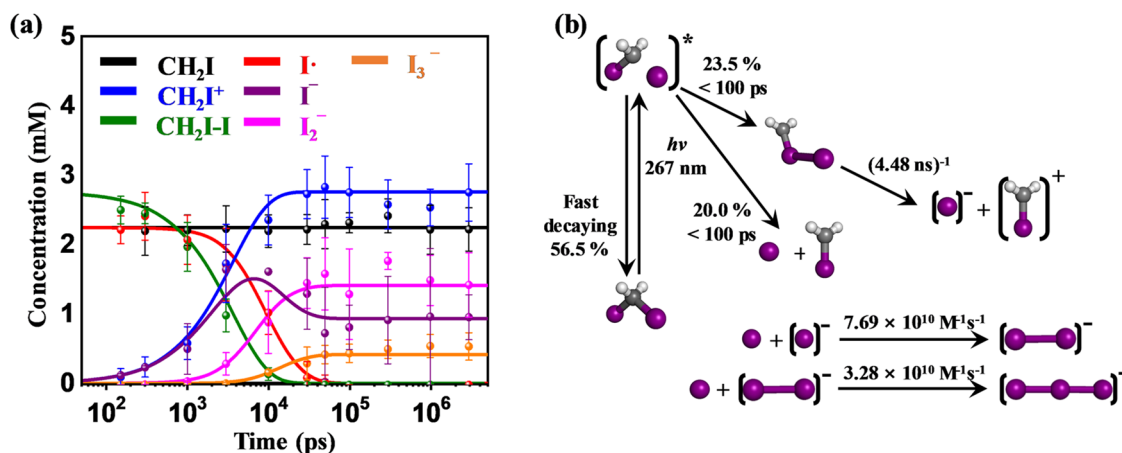


FIG. 4. (a) Time-dependent concentrations of chemical species involved in the photodissociation of CH₂I₂ in methanol based on the heterolysis model and (b) its overall reaction mechanism.

performed quantum chemical calculations for a series of iodine compounds, CH_2I_2 , CHI_3 , and $\text{C}_2\text{H}_4\text{I}_2$, each of which generates an isomer containing an I–I bond via photodissociation, and their isomers in the environment of a polar solvent. In particular, from the quantum chemical calculations, we obtained the dipole moment values of 8.89 D, 13.32 D, and 2.40 D for the $\text{CH}_2\text{I-I}$, $\text{CHI}_2\text{-I}$, and $\text{C}_2\text{H}_4\text{I-I}$ isomers, respectively. Also, the partial charge at the terminal I atom of the I–I group of each isomer was examined and their values were calculated to be -0.571 , -0.671 , and -0.073 for $\text{CH}_2\text{I-I}$, $\text{CHI}_2\text{-I}$, and $\text{C}_2\text{H}_4\text{I-I}$, respectively. According to the chemical intuition of electronegativity, a molecule of higher polarity should have higher probability of undergoing heterolysis, especially in a polar solvent like methanol. Therefore, we can infer that the probability of heterolysis becomes higher for the isomers with higher dipole moment and higher partial charge at the terminal I atom, that is, in the order of $\text{CHI}_2\text{-I} > \text{CH}_2\text{I-I} > \text{C}_2\text{H}_4\text{I-I}$.

This predicted order of reactivity for the three isomers is consistent with the energetics of the heterolysis reactions for the three isomers calculated with a DFT method (MN12-SX/AVTZ), that is, higher energy is required for the endothermic heterolysis reaction in the order of $\text{CHI}_2\text{-I} < \text{CH}_2\text{I-I} < \text{C}_2\text{H}_4\text{I-I}$, as shown in Fig. S4. First, it should be noted that the $\text{C}_2\text{H}_4\text{I-I}$ isomer has a bridged conformation, which has a relatively high symmetry compared with the structures of the other isomers, in both polar³² and nonpolar¹¹ solvents according to previous TRXL studies and, as a result, $\text{C}_2\text{H}_4\text{I-I}$ has a much smaller dipole moment than those of the other isomers, thus making it difficult for the heterolysis to occur. Accordingly, the heterolysis of $\text{C}_2\text{H}_4\text{I-I}$ is an endothermic reaction that requires the highest energy among the heterolysis reactions of the three isomers (see Fig. S4). Also, the heterolysis of $\text{C}_2\text{H}_4\text{I-I}$ (114.6 kJ/mol) is energetically unfavorable compared with its dissociation into C_2H_4 and I_2 (13.3 kJ/mol), and therefore, it does not occur.

By contrast, $\text{CHI}_2\text{-I}$ has the largest dipole moment among the three isomers and therefore the heterolysis of $\text{CHI}_2\text{-I}$ should occur most easily among the three isomers, which is supported by the smallest reaction energy required for the heterolysis of $\text{CHI}_2\text{-I}$ as shown in Fig. S4. However, any signature of the negative ionic species (I_2^- and I_3^-) was not observed in a previous study on the photodissociation of CHI_3 in methanol using TRXL and time-resolved X-ray absorption spectroscopy.^{28,34} In fact, in that same study, the $\text{CHI}_2\text{-I}$ isomer was not observed, either, within the signal-to-noise ratio of those measurements. While there was a time-resolved spectroscopic study that reported the formation of the $\text{CHI}_2\text{-I}$ isomer,^{29–31,35} the absence of such signature in the X-ray scattering and absorption signals, which are sensitive to molecular structure and of which the intensities are proportional to the populations of chemical species, indicates that the formation of the $\text{CHI}_2\text{-I}$ isomer must be a minor reaction pathway, at best, for the photodissociation of CHI_3 in methanol. Therefore, despite the high polarity of the $\text{CHI}_2\text{-I}$ isomer, the negative ionic photoproducts such as I_2^- and I_3^- may not be observed in the photodissociation of CHI_3 due to a low yield of the $\text{CHI}_2\text{-I}$ isomer not because of the low probability of the $\text{CHI}_2\text{-I}$ isomer undergoing the heterolysis. Conversely, despite the high probability of heterolysis for $\text{CHI}_2\text{-I}$, the absence of the negative ionic species (I_2^- and I_3^-) in the photodissociation of CHI_3 can serve as another evidence that supports the very low yield of the $\text{CHI}_2\text{-I}$ isomer proposed in the previous TRXL study.^{28,34}

Thus, we can conclude that the heterolysis occurs only for the $\text{CH}_2\text{I-I}$ isomer, which has high polarity and is produced with a high yield.

CONCLUSIONS

In this study, we investigated the photodissociation dynamics of CH_2I_2 in methanol using TRXL and unveiled the mechanism and the origin of the formation of I_2^- and I_3^- , which are observed only in CH_2I_2 but not in other iodine-containing compounds such as CHI_3 , $\text{C}_2\text{H}_4\text{I}_2$, I_2 , I_3^- , and $\text{C}_2\text{F}_4\text{I}_2$. The analysis of our TRXL data supports that *iso*- $\text{CH}_2\text{I-I}$ is decomposed via heterolysis into CH_2I^+ and I^- and subsequently I^- undergoes nongeminate recombination with I^{\cdot} to form I_2^- and I_3^- . Based on the findings of this work, we propose that the high polarity of the *iso*- $\text{CH}_2\text{I-I}$ isomer and its subtle interaction with the polar solvent are responsible for the unique photochemistry of CH_2I_2 in the polar solvent, that is, the formation of negative ionic products such as I_2^- and I_3^- via heterolysis. The photodissociation of CH_2I_2 is a good example showing the dramatic effect of the complex and delicate solute-solvent interaction on the outcome of a chemical reaction.

EXPERIMENTAL PROCEDURES

The TRXL experiment conducted as part of this study was performed at the NW14A beamline in the High Energy Accelerator Research Organization (KEK). The full methods including the DFT calculations, MD simulations, global fit analysis, and TRXL setups are provided in the [supplementary material](#).

SUPPLEMENTARY MATERIAL

The [supplementary material](#) contains detailed methods and data acquisition, data processing, global fit analysis, molecular dynamics simulation for the solute-solvent cross term, computational details, sine-Fourier transform, and Figs. S1–S5.

ACKNOWLEDGMENTS

This work was supported by the Institute for Basic Science (No. IBS-R004). This work was performed under the approval of the Photon Factory Program Advisory Committee (Proposal No. 2014G123). This work was supported by the Basic Science Research Program through the National Research Foundation of Korea (NRF) funded by the Ministry of Science, ICT and Future Planning (Grant Nos. NRF-2016R1E1A1A01941978 and NRF-2016R1D1A1B03933120). This work was also supported by JSPS KAKENHI Grant Number 17H06438 in Scientific Research on Innovative Areas “Innovations for Light-Energy Conversion (I4LEC)”.

The authors declare no competing financial interests.

REFERENCES

- 1 A. S. Rury, T. E. Wiley, and R. J. Sension, *Acc. Chem. Res.* **48**, 860 (2015).
- 2 J. H. Lee, M. Wulff, S. Bratos, J. Petersen, L. Guerin, J. C. Leicknam, M. Cammarata, Q. Kong, J. Kim, K. B. Møller, and H. Ihee, *J. Am. Chem. Soc.* **135**, 3255 (2013).
- 3 V. A. Apkarian and N. Schwentner, *Chem. Rev.* **99**, 1481 (1999).
- 4 B. D. Smith, K. G. Spears, and R. J. Sension, *J. Phys. Chem. A* **120**, 6575 (2016).

- ⁵D. A. Braden, E. E. Parrack, and D. R. Tyler, *Coord. Chem. Rev.* **211**, 279 (2001).
- ⁶J. Yao, H. S. Im, M. Foltin, and E. R. Bernstein, *J. Phys. Chem. A* **104**, 6197 (2000).
- ⁷M. S. Zakerhamidi, A. Ghanadzadeh, H. Tajalli, M. Moghadam, M. Jassas, and R. Hosseini Nia, *Spectrochim. Acta, Part A* **77**, 337 (2010).
- ⁸B. Gilbert, J. E. Katz, N. Huse, X. Zhang, C. Frandsen, R. W. Falcone, and G. A. Waychunas, *Phys. Chem. Chem. Phys.* **15**, 17303 (2013).
- ⁹K. H. Kim, H. Ki, J. H. Lee, S. Park, Q. Kong, J. Kim, J. Kim, M. Wulff, and H. Ihee, *Phys. Chem. Chem. Phys.* **17**, 8633 (2015).
- ¹⁰K. H. Kim, J. H. Lee, J. Kim, S. Nozawa, T. Sato, A. Tomita, K. Ichianagi, H. Ki, J. Kim, S. I. Adachi, and H. Ihee, *Phys. Rev. Lett.* **110**, 165505 (2013).
- ¹¹J. Kim, J. H. Lee, J. Kim, S. Jun, K. H. Kim, T. W. Kim, M. Wulff, and H. Ihee, *J. Phys. Chem. A* **116**, 2713 (2012).
- ¹²C. W. Ahn, H. Ki, J. Kim, J. Kim, S. Park, Y. Lee, K. H. Kim, Q. Kong, J. Moon, M. N. Pedersen, M. Wulff, and H. Ihee, *J. Phys. Chem. Lett.* **9**, 647 (2018).
- ¹³A. N. Tarnovsky, V. Sundstrom, E. Åkesson, and T. Pascher, *J. Phys. Chem. A* **108**, 237 (2004).
- ¹⁴A. N. Tarnovsky, J.-L. Alvarez, A. P. Yartsev, V. Sundström, and E. Åkesson, *Chem. Phys. Lett.* **312**, 121 (1999).
- ¹⁵K. I. Saitow, Y. Naitoh, K. Tominaga, and K. Yoshihara, *Chem. - Asian J.* **3**, 696 (2008).
- ¹⁶X. Guan, X. Lin, W. M. Kwok, Y. Du, Y. L. Li, C. Zhao, D. Wang, and D. L. Phillips, *J. Phys. Chem. A* **109**, 1247 (2005).
- ¹⁷X. Zheng and D. L. Phillips, *J. Phys. Chem. A* **104**, 6880 (2000).
- ¹⁸W. M. Kwok, C. Ma, A. W. Parker, D. Phillips, M. Towrie, P. Matousek, X. Zheng, and D. L. Phillips, *J. Chem. Phys.* **114**, 7536 (2001).
- ¹⁹Y. L. Li, D. Wang, K. H. Leung, and D. L. Phillips, *J. Phys. Chem. A* **106**, 3463 (2002).
- ²⁰J. Vincent, M. Andersson, M. Eklund, A. B. Wöhri, M. Odelius, E. Malmerberg, Q. Kong, M. Wulff, R. Neutze, and J. Davidsson, *J. Chem. Phys.* **130**, 154502 (2009).
- ²¹J. Davidsson, J. Poulsen, M. Cammarata, P. Georgiou, R. Wouts, G. Katona, F. Jacobson, A. Plech, M. Wulff, G. Nyman, and R. Neutze, *Phys. Rev. Lett.* **94**, 245503 (2005).
- ²²D. C. Blomstrom, K. Herbig, and H. E. Simmons, *J. Org. Chem.* **30**, 959 (1965).
- ²³P. J. Kropp, *Acc. Chem. Res.* **17**, 131 (1984).
- ²⁴M. Odelius, M. Kadi, J. Davidsson, and A. N. Tarnovsky, *J. Chem. Phys.* **121**, 2208 (2004).
- ²⁵P. M. Kroger, P. C. Demou, and S. J. Riley, *J. Chem. Phys.* **65**, 1823 (1976).
- ²⁶M. Kawasaki, S. J. Lee, and R. Bersohn, *J. Chem. Phys.* **63**, 809 (1975).
- ²⁷K. H. Kim, J. Kim, J. H. Lee, and H. Ihee, *Struct. Dyn.* **1**, 011301 (2014).
- ²⁸K. H. Kim, J. Kim, K. Y. Oang, J. H. Lee, D. Grolimund, C. J. Milne, T. J. Penfold, S. L. Johnson, A. Galler, T. W. Kim, J. G. Kim, D. Suh, J. Moon, J. Kim, K. Hong, L. Guérin, T. K. Kim, M. Wulff, C. Bressler, and H. Ihee, *Phys. Chem. Chem. Phys.* **17**, 23298 (2015).
- ²⁹X. Zheng and D. L. Phillips, *Chem. Phys. Lett.* **324**, 175 (2000).
- ³⁰Y. L. Li, D. M. Chen, D. Wang, and D. L. Phillips, *J. Org. Chem.* **67**, 4228 (2002).
- ³¹M. Wall, A. N. Tarnovsky, T. Pascher, V. Sundström, and E. Åkesson, *J. Phys. Chem. A* **107**, 211 (2003).
- ³²H. Ihee, M. Lorenc, T. K. Kim, Q. Kong, M. Cammarata, J. H. Lee, S. Bratos, and M. Wulff, *Science* **309**, 1223 (2005).
- ³³H. L. Jae, K. K. Tae, J. Kim, Q. Kong, M. Cammarata, M. Lorenc, M. Wulff, and H. Ihee, *J. Am. Chem. Soc.* **130**, 5834 (2008).
- ³⁴J. H. Lee, J. Kim, M. Cammarata, Q. Kong, K. H. Kim, J. Choi, T. K. Kim, M. Wulff, and H. Ihee, *Angew. Chem., Int. Ed.* **47**, 1047 (2008).
- ³⁵P. Z. El-Khoury, W. M. Kwok, X. Guan, C. Ma, D. L. Phillips, and A. N. Tarnovsky, *ChemPhysChem* **10**, 1895 (2009).
- ³⁶K. Ichianagi, T. Sato, S. Nozawa, K. H. Kim, J. H. Lee, J. Choi, A. Tomita, H. Ichikawa, S. Adachi, H. Ihee, and S. Koshihara, *J. Synchrotron Radiat.* **16**, 391 (2009).
- ³⁷F. Weigend and A. Baldes, *J. Chem. Phys.* **133**, 174102 (2010).
- ³⁸C. Tao, C. Mukarakate, Y. Mishchenko, D. Brusse, and S. A. Reid, *J. Phys. Chem. A* **111**, 10562 (2007).
- ³⁹C. Tao, C. Mukarakate, and S. A. Reid, *J. Am. Chem. Soc.* **128**, 9320 (2006).
- ⁴⁰K. H. Kim, H. Ki, K. Y. Oang, S. Nozawa, T. Sato, J. Kim, T. K. Kim, J. Kim, S. I. Adachi, and H. Ihee, *ChemPhysChem* **14**, 3687 (2013).